Indentation strain burst phenomenon induced by grain boundaries in niobium

M.G. Wang
Department of Mechanical Engineering, The University of Hong Kong, Pokfulam Road, Hong Kong, People's Republic of China; and College of Science, Northeastern University, Shenyang 110006, People's Republic of China

A.H.W. Ngan[a)]
Department of Mechanical Engineering, The University of Hong Kong, Pokfulam Road, Hong Kong, People's Republic of China

(Received 8 February 2004; accepted 20 May 2004)

Using depth-sensing indentation, a pop-in phenomenon induced by grain boundaries, namely, a sudden indenter displacement jump when indented near a grain boundary segment, was observed in polycrystalline niobium. This grain-boundary type of pop-in occurs at a larger force than the initial elasto-plastic pop-in, which is observed with and without a grain boundary nearby. The experimental results show that this pop-in effect has a close relationship with the misorientation across the grain boundary. The occurrence of this pop-in phenomenon is rationalized in terms of slip transmission across the grain boundary.

I. INTRODUCTION

Numerous previous attempts have been made in the past to use subgranular microhardness indentation to probe the hardening behavior of grain boundaries in bicrystals or large-grained polycrystalline specimens.[1–8] Whether hardness, which is defined as the indentation load divided by the area of the indent made, can be a sensitive enough parameter to represent the hardening potential of a grain boundary, however, is controversial. In many reports where an increase in the measured hardness was observed, the grain boundary hardening was attributed to segregation of impurity atoms. Examples of these include doped zone-refined metals such as Pb, Sn and Zn,[1] tin segregation in alpha iron–tin alloy,[2] calcium segregation in NaCl bicrystals,[3] and in niobium bicrystals.[4,5] In these experiments, proper heat treatment procedures were followed to achieve enough segregation of impurities at grain boundaries.

In other works, the observed grain boundary hardening was attributed to the difficulty in slip transmission across grain boundaries. From macroscopic tensile tests on high-purity aluminium, Wyrzykowski and Grabski[6] concluded that the Hall–Petch slope k_y depends on the distribution function of the grain boundary diffusivity, indicating a dependence of k_y on the grain boundary structure. Lee et al.[7] observed larger grain boundary hardening effects from microhardness measurements in undoped Ni_3Al than in boron-doped Ni_3Al, and by referencing to bulk deformation of polycrystalline samples in which a higher Hall–Petch slope is observed in the undoped situation, these authors concluded that a link exists between the degree of grain boundary hardening and the ease of slip transmission across grain boundaries. However, in a recent study by Wo and Ngan,[8] an increase in the measured hardness near grain boundaries was not observed in depth-sensing indentation (more commonly known as nanoindentation) experiments on undoped Ni_3Al. Careful scanning electron microscopy (SEM) and atomic force microscopy (AFM) observation of the indents made near a grain boundary and far away from a grain boundary within the same grain using the same load showed identical shape and size. These results raise the question of whether hardness is a sensitive enough parameter to represent the slip transmission potential of a grain boundary.

To clarify the effects of a grain boundary on slip transmission, we performed depth-sensing indentation near grain boundaries in polycrystalline niobium. We choose to study niobium here because it has body-centered-cubic (bcc) crystal structure. The bcc metals are well-known to exhibit much higher Hall–Petch slope compared to face-centered-cubic metals and so in the case of bcc, resistance to intergranular slip transmission is expected to be much more prominent.

II. EXPERIMENTAL PROCEDURE

In the present work, a slug of niobium with 99.99% purity was purchased from the Alfa Aesar Company

[a)]Address all correspondence to this author.
e-mail: hwngan@hkucc.hku.hk
DOI: 10.1557/JMR.2004.0316

(Ward Hill, MA). This sample was made by an electron-beam melting method. Cylindrical specimens with a 6.35 mm diameter and 5 mm length were cut from the niobium rod. These specimens were then annealed for 20 days at a temperature of 1200 °C in a vacuum of approximately 10^{-5} Torr, followed by furnace cooling to room temperature. The resultant grain size was 500 ± 200 μm. Each of the annealed samples was mechanically ground using 600-grade emery paper and then electropolished for 2–5 min in a solution containing one part of HF and nine parts of H_2SO_4 in volume. To reveal the grain boundary, the samples were etched in an etchant containing 60 ml HF (48% concentration), 40 ml H_2O_2 (30% concentration), and 0.55 g NaF, for about 10–20 s. This etchant is a modification of that used by Baranova.[9]

Indentation tests were performed with a CSM Instruments SA (Peseux, Switzerland) indenter using a simple loading-holding-unloading profile with a maximum force of 30 to 50 mN. A Berkovich indenter was used for making indents along selected grain boundaries on the Nb sample. The indenter was loaded and unloaded at a constant rate of 30 mN/min, and the peak load was held for 10 s before unloading. The impressions were examined by backscattered imaging by either a Cambridge Stereoscan 360 or a 440 scanning electron microscope (Cambridge, UK). The orientations of the grains were determined by electron backscattering patterns (EBSP) using a LEO 1530 (LEO Elektronenmikroskopie GmbH, Oberkochen, Germany) field-emission SEM. The EBSPs were recorded by means of a low-light charge coupled device (CCD) video camera. The EBSD data were analyzed by the software HKL-Channel-5. Topographical profiles around the indents were measured quantitatively using tapping mode AFM on a Thermomicroscopes scanning probe microscope.

In analyzing the data, the selected grain boundary segments were assumed to be perpendicular to the sample free surface. Since grains with sectional dimensions of larger than 300 μm were always selected for indentation, and the Berkovich indenter is in fact a very blunt indenter with an apex angle of 140.6°, the grain boundaries were highly unlikely to develop sharp curvatures within a depth of only about 1 μm below the surface and to be intersected by the indenter below the surface.

III. RESULTS

A. Pop-in due to grain boundaries

An interesting effect of grain boundary on the depth-sensing indentation behavior was observed in the present experiments. Figure 1 shows the load versus displacement curves of two indents made in the same grain but at two different distances from a given grain boundary. One indent was situated at 3.82 μm from the grain boundary [Fig. 1(a)], and the other was at 6.81 μm from it. It can

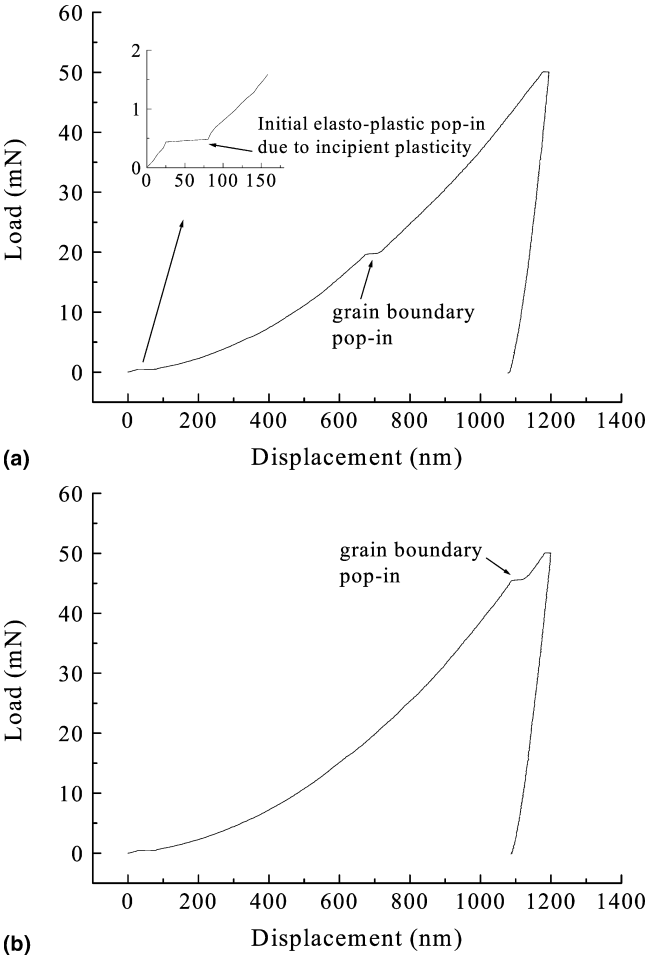

FIG. 1. Load–displacement curves showing the grain boundary pop-in in two indents made within the same grain. The applied maximum load is 50 mN in both cases. (a) The distance from the indent center to the nearby grain boundary is 3.82 μm, and the load at which the grain boundary pop-in occurs is 19.47 mN. (b) The distance from indent center to the nearby grain boundary is 6.81 μm, and the load at which the grain boundary pop-in occurs is 45.52 mN.

be seen that in each of the two curves, there are two strain bursts. The first of these occurs at about 0.45 mN, and this pop-in happens in all the indentations no matter they are made close to or far away from grain boundaries. This pop-in is likely to be due to incipient plasticity as the crystal deformation transits from being elastic to plastic.[10–17] In other locations, incipient plasticity was sometimes observed to occur in the form of the so-called "staircase" phenomenon,[13] in which a series of smaller multiple pop-ins followed the first major pop-in. The staircase phenomenon is frequently observed in other bcc crystals,[13] and in the case of Nb here, it usually dies down at loads larger than ~5mN and the displacement jumps concerned are usually a few nanometers. In what follows, we focus on the second major pop-in in the curves in Fig. 1, which were observed only in indentations made close enough to a grain boundary. This type of pop-in found near a grain boundary usually had much

larger displacement jumps than the staircase type, and can therefore be unambiguously identified. Also, the load at which this grain-boundary pop-in occurs is found to depend on the distance of the indent from the grain boundary. In Fig. 1(a), in which the indent is closer to the grain boundary, the second pop-in occurs at a load of 19.47 mN, while in Fig. 1(b), in which the indent is further away, the second pop-in occurs at a higher load of 45.53 mN. In Fig. 2 the load at which the grain-boundary pop-in occurs is plotted as a function of the distance between the indent center and a grain boundary. Here, the data are taken from indentations made within the same grain and near the same grain boundary (as in Fig. 1), and so the crystal orientation factor is common amongst all the data plotted. A clear trend of increasing pop-in load as the distance from the grain boundary increases is evident. Table I shows an analysis of the same set of data. Here, the radius of the elasto-plastic boundary is estimated using the equation

$$c = \sqrt{\frac{3P}{2\pi\sigma_{ys}}} \quad , \tag{1}$$

proposed by Kramer et al.[18] In this equation, P is the indentation load (here the pop-in load), and σ_{ys} is the yield strength. Although it was proposed as an approximate model, recent transmission electron microscopy experiments by Chiu and Ngan[17] in Ni_3Al confirmed the validity of this equation in predicting the plastic zone size c. For Nb, the yield strength $\sigma_{ys} = 103$ MPa,[19] and the calculated values of c are shown in Table I for the grain boundary segment with which Figs. 1 and 2 are concerned. An interesting observation from Table I is that the ratio c/d, where d is the distance of the indent from the grain boundary, scatters within a narrow range around 2 for the grain boundary segment concerned. However, the size δ_{exc} of the pop-in exhibits no systematic relation with the pop-in load or the distance from the grain boundary.

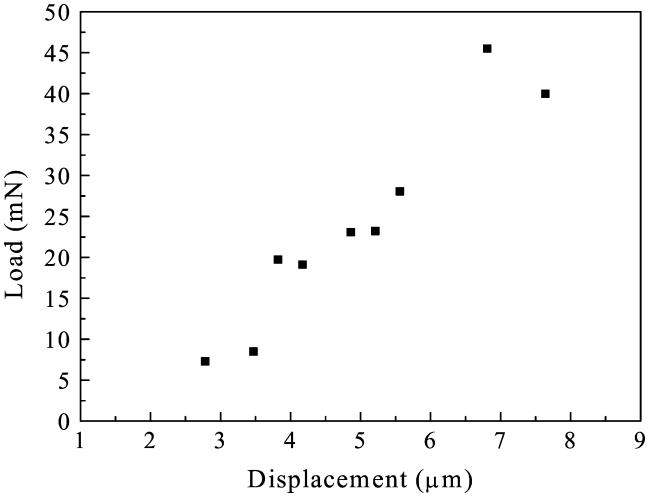

FIG. 2. Load at which grain boundary pop-in occurs versus distance of the indent center to the grain boundary. Data are from indentations made within the same grain near the same grain boundary (labeled as "1" in Table II). The applied maximum load is 50 mN. The distances from the indent center to grain boundary were measured from SEM images.

The ratio c/d was also calculated from the pop-in data obtained near other grain boundaries. While this ratio is quite constant for a selected grain boundary segment, it can vary amongst different grain boundaries, and Fig. 3 shows a plot of the statistical distribution of this ratio from the pop-in data collected from different grain boundaries. It is evident that the pop-in phenomenon occurs mostly at $c/d \approx 2$. The number of grain-boundary pop-in with higher c/d ratios is lower, and no grain-boundary pop-in was observed with a c/d ratio exceeding 5 or less than 1.5. The experimental results, in fact, indicate that although the pop-in load can vary depending on the distance from the grain boundary as well as the grain boundary concerned, the ratio c/d still remains at a nearly constant value when the indentation is made near a given grain boundary segment. This shows the ratio c/d is relevant to the properties of the grain boundary rather than the load applied.

To see the effects of grain boundary misorientation on the observed grain-boundary induced pop-in, the occurrence of the grain boundary pop-in up to the maximum applied load of 50 mN is compared with the misorientation. The latter is quantified by the factor

$$m' = \cos(\theta_A)\cos(\theta_B) \quad , \tag{2}$$

where θ_A is the angle between the closest {110} or {112} slip planes in the two adjacent grains, and θ_B is the angle between the closest ⟨111⟩ slip directions on the closest slip planes.[8] Table II shows the relationship between m' and the occurrence of the pop-in in a number of grain boundaries studied. Here, the indentations made were situated within 10 μm from the grain boundaries concerned, and at such short distances, a grain-boundary pop-in, if present, would be detected within the maximum load of 50 mN. The grain orientations were determined from EBSP, and the coincidence site lattice (CSL) of any special misorientation relationship was also determined and is given Table II. It can be seen from Table II that the pop-in phenomenon occurs when the m' value is above approximately 0.9. Since a higher m' value corresponds to better alignment of the slip systems on either side of the grain boundary, the observation here suggests that the grain-boundary pop-in is related to the ease of slip transmission across the grain boundary. The specialty of the grain boundary in terms of the CSL, on the other hand, has no apparent effect since grain boundary 4 and 5 in Table II have similar CSL, but the occurrence of pop-in is different.

TABLE I. Data for grain boundary pop-in obtained from different indentations made in the same grain near the same grain boundary segment. The elasto-plastic boundary is calculated as $c = \sqrt{3P/2\pi\sigma_{ys}}$ (see text).

Distance d from the indent center to grain boundary (μm)	Load P at which grain-boundary pop-in occurs (mN)	Elasto-plastic boundary c from indent center	c/d	Pop-in size, δ_{exc} (nm)
2.78	7.30	5.82	2.09	31.08
3.47	8.50	6.28	1.81	17.16
3.82	19.47	9.57	2.50	37.62
4.17	19.13	9.42	2.26	36.16
4.86	23.09	10.35	2.13	13.58
5.21	23.22	10.38	1.99	32.09
5.56	28.07	11.41	2.05	19.81
6.81	45.53	14.53	2.13	33.85
7.64	40.00	13.62	1.78	19.34

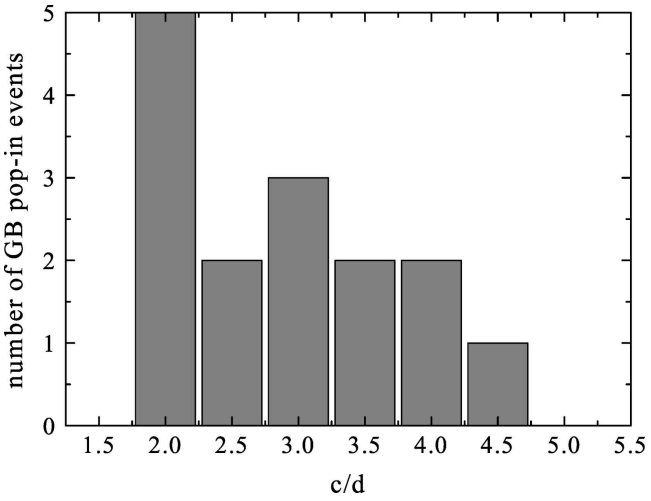

FIG. 3. Statistical distribution of the c/d ratio for grain-boundary pop-in for different grain boundaries.

B. Indent topography

The key questions to be answered here are (i) whether the hardness is influenced by the occurrence of a grain-boundary pop-in, and (ii) whether the hardness suffers a change near a grain boundary. To remove the effects of thermal drift and specimen creep, the hardness was measured in this work by direct imaging of the indent geometry using SEM after the indentation. Figure 4 shows a SEM image of three nearby indents made close to a grain boundary using the same load of 50 mN. One of these indents exhibited pop-in while the other two did not. Since all three indents were quite close to the same grain boundary segment, the slip transfer potential, or critical c/d ratio, of the grain boundary portions probed by the three indents should be quite similar, and this explains why the two indents in Fig. 4 with slightly larger distance d did not exhibit the pop-in. It can be seen that the sizes and shapes of all three indents are practically identical, and hence their hardness values are essentially identical, considering the magnitude of measurement errors. In fact, at approximately 50 mN, the excursion length Δh is typically about 10–30 nm. According to the ideal area function of a Berkovich tip $A_c = 24.5\ h_c^2$, where A_c is the contact area and h_c the contact depth, if $\Delta h_c \approx \Delta h =$ 30 nm (maximum value) and $h_c = 1000$ nm, then $\Delta A_c = 49\ h_c\ \Delta h_c = 1.5\ \mu m^2$. From the SEM image of the indent, $A_c \sim 24.5\ \mu m^2$, and the average measurement error of the projected indent area A_c is about $\pm 1\ \mu m^2$. Therefore, the anticipated area change produced by the grain-boundary pop-in is not significantly larger than the measurement error of area using SEM, and hence the occurrence of the pop-in is not expected to yield an observable reduction in hardness.

This expectation is confirmed by the results presented in Fig. 5, which shows the measured hardness as a function of the distance from the indent center to a grain boundary. The maximum applied load is 50 mN. Here, the hardness values are calculated according to the definition of indentation load divided by the projected area of the indent. The indentation load used was the value detected by the nanoindenter, which was usually deviated within ± 0.6 mN from the preset value. The projected indent area was measured from the post-indentation SEM images of the indents. The error mainly comes from measurement of indent projected area A_c due to pile-up or sink-in effect. For niobium metal, the pile-up effect is not considerable at 50 mN, and the average measurement error of the projected indent area A_c is about $\pm 1\ \mu m^2$. As a result, the measurement error of the hardness value H is about ± 0.04 GPa at 50 mN. From Fig. 5, it is seen that, when the indent is made at a distance from the grain boundary farther than 9 μm, no grain-boundary induced pop-in occurs for this grain boundary. Moreover, the measured hardness does not show any statistically significant difference in the range of error irrespective of whether there is a grain-boundary pop-in.

Figure 6 shows the backscattered SEM images of four indents in a niobium sample, the surface of which was

TABLE II. Relationship between grain boundary misorientation and pop-in. $m' = \cos(\theta_A)\cos(\theta_B)$. θ_A is the angle between the closest slip planes in the two adjacent grains, and θ_B is the angle between the closest slip directions on the closest slip planes. CSL denotes coincidence site lattice, and blank entries mean corresponding grain boundaries are not CSL boundaries.

Grain boundary number	CSL Σ	$\cos(\theta_A)$	$\cos(\theta_B)$	m'	Grain boundary pop-in
1		0.9970	0.9948	0.9918	Yes
2		0.9953	0.9913	0.9866	Yes
3		0.9946	0.9617	0.9665	Yes
4	41c	0.9953	0.9404	0.9360	Yes
5	41b	0.9976	0.8879	0.8858	No
6	9	0.9972	0.8858	0.8833	No
7	29b	0.9972	0.8339	0.8316	No
8		0.9966	0.8143	0.8115	No

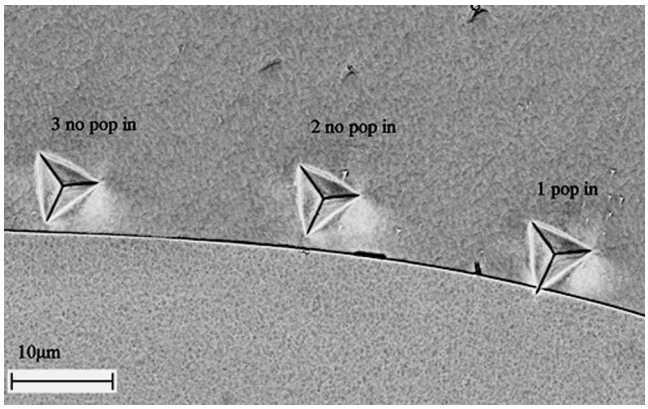

FIG. 4. SEM image of three nearby indents made near a grain boundary at 50 mN. Indent 1 has a secondary pop-in occurred while indents 2 and 3 do not have secondary pop-in at mN-scale loads.

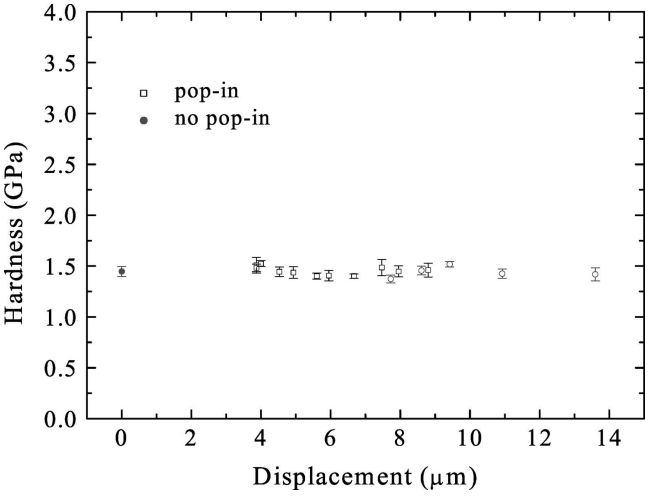

FIG. 5. Hardness versus distance from indent center to grain boundary. The maximum applied load is 50 mN.

identified to be near (310) through EBSP measurement. At a lower load such as 50 mN, no significant pile-up or obvious slip traces were observed around the indent. However, when the load was increased up to 300 mN, the SEM images of the indents shows clear slip traces, typically spreading over a distance comparable with the size of the indent. Although no clear slip traces were observed in the SEM image at 50 mN, the backscattered SEM images in Fig. 6 can help identify the extent of lattice rotation around the indents. The indents in Figs. 6(a)–6(d) were made on the same grain in a niobium sample. In Figs. 6(a) and 6(c), both indents were very close to a grain boundary, and grain-boundary pop-ins were identified from the load-displacement curves of these two indents. In Figs. 6(b) and 6(d), the indents were in the grain interior and farther from the grain boundary respectively, and no pop-in was detected for these two indents. Although the indents in Figs. 6(c) and 6(d) are situated at similar distances from the grain boundary segments concerned, the fact that pop-in is observed in Fig. 6(c) but not in Fig. 6(d) implies that the two grain boundary segments have very different potential to transmit slip, i.e., very different critical *c/d* ratios. Careful inspection of these SEM images shows that the regions with brighter contrast encircled by dotted lines near the grain boundary in Figs. 6(a) and 6(c) are larger than the corresponding regions in Figs. 6(b) and 6(d). Since the contrast in a backscattered SEM image is due to differences in lattice rotation, comparing Figs. 6(a) and 6(d) shows that the deformation is perhaps more severe near a grain boundary in the cases of Figs. 6(a) and 6(c) than the cases in Figs. 6(b) and 6(d), in which the grain boundary is farther away. Despite the difference in lattice rotations surrounding the indents, all the indents in Figs. 6(a)–6(d) have the same size and shape. This again points to the conclusion that a variation of hardness due to proximity to a grain boundary is not observed beyond possible doubts arising from experimental errors. A similar conclusion is reached in polycrystalline Ni_3Al recently by Wo and Ngan.[8]

IV. DISCUSSION

The observation of more severe lattice deformation in the gap between an indent and a grain boundary as seen

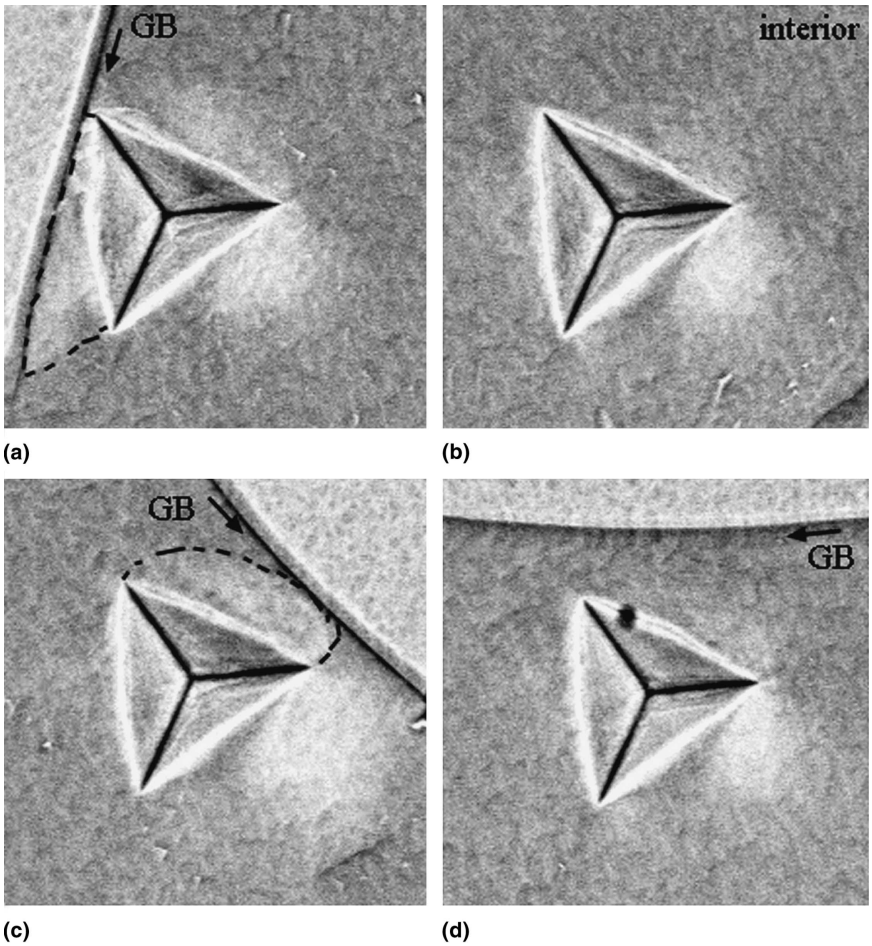

FIG. 6. Backscattered SEM images of indents made using a load of 50mN: (a) indent showing grain-boundary pop-in near a grain boundary, (b) an indent within grain interior, (c) an indent showing grain-boundary pop-in near a grain boundary, and (d) an indent near a grain boundary but not showing grain-boundary pop-in.

in Fig. 6(a) and 6(c) indicates that the grain boundary blocks the propagation of deformation into the next grain. A build-up of stress in this gap is therefore expected, and this could trigger some stress-relief mechanism. There can be two possible stress relief mechanisms that can be related to the observed grain-boundary pop-in, namely, (i) grain boundary cracking, and (ii) incipient plasticity in the grain next to the indented grain. Figure 7 shows the AFM image of a typical indentation exhibiting a grain boundary pop-in during the loading process. This image was taken using a sharp Si_3N_4 AFM tip in the tapping mode. It can be seen from the line scan across the indent that, within the resolution of the AFM technique, no cracking of the grain boundary seems to have occurred. There is therefore no evidence supporting grain boundary cracking as a possible cause for the present observed pop-in.

The misorientation factor m' in Eq. (2) above measures the alignment of the slip systems on either side of the grain boundary. A higher value of m' denotes better alignment and hence easier slip transmission across the grain boundary. The results in Table II indicate clearly that for grain boundaries with easier slip transmission (higher m'), the grain-boundary induced pop-in occurs at a lower load, i.e., within the maximum load of 50 mN applied, and for grain boundaries across which slip transmission is difficult (lower m'), no pop-in is observed up to the maximum load. This observation suggests that the pop-in is due to slip transmission across the grain boundary, i.e., incipient plasticity in the grain next to the indented grain. This conclusion is further supported by the observation from Table I and Fig. 3 in that at the load at which the pop-in occurs, the c/d ratio is within a narrow range between 1.5 and 5.

A rough analysis can be performed to predict the condition at which a pop-in occurs within the incipient plasticity interpretation. The stress state within the plastic zone underneath the indenter is very complicated, although for macro-indents simplified continuum-plasticity models such as the cavity model are found to be reasonably accurate.[20] However, previous analyses by Kramer et al.,[18] and Chiu and Ngan[17] have shown that the

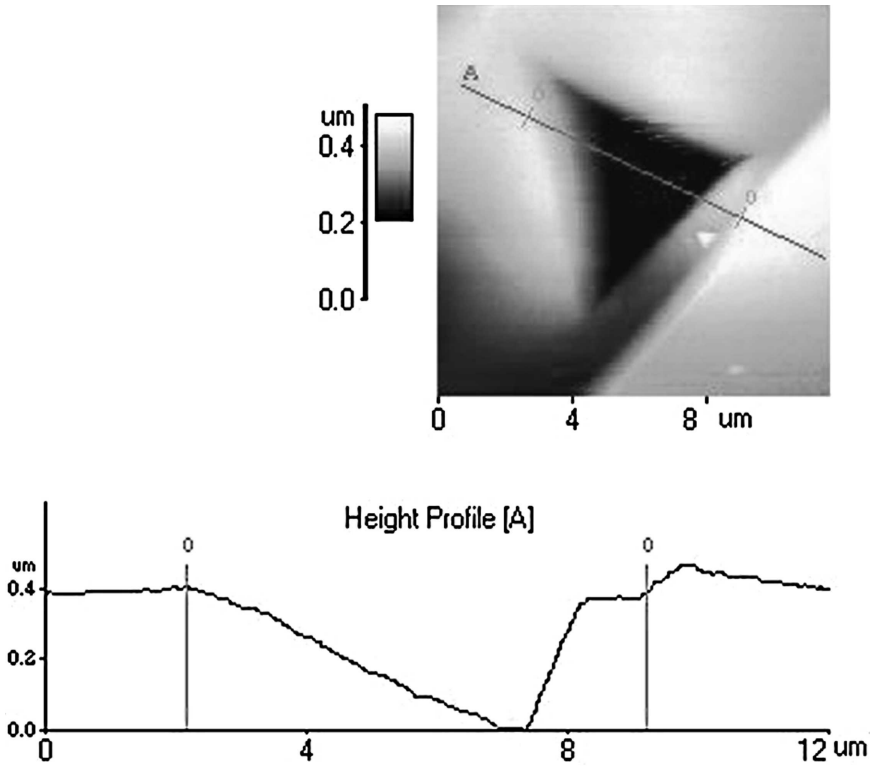

FIG. 7. Tapping mode AFM image of an indentation showing the grain boundary pop-in. The indentation was loaded to a maximum load of 50 mN.

position of the elasto-plastic boundary in the submicronindentation situation can be accurately described by Eq. (1), which was derived by Kramer et al.[18] using the equations for the elastic region in the cavity model. Chiu and Ngan[17] have furthermore compared the predictions of other models including the finite element model by Zeng et al.,[21] the Hertzian contact model, a uniform pressure contact model, as well as a flat punch contact model, and have found that all these elastic models predict nearly the same elasto-plastic boundary as the cavity model. Determination of the elasto-plastic boundary by TEM also confirms the validity of Eq. (1). In essence, these analyses support the simple picture that the plastic field details within and near the indent core do not influence the far field elastic region, and hence the latter is well described by any elastic models which differ only in terms of the actual contact geometry between the tip and the specimen. For this reason, we can believe that the elastic region outside the elasto-plastic boundary (Fig. 8) can be described by the following equations from the cavity model:[20]

$$\sigma_r = -\frac{2\sigma_{ys}}{3}\left(\frac{c}{r}\right)^3,\ \sigma_\theta = \frac{\sigma_{ys}}{3}\left(\frac{c}{r}\right)^3,\ \text{and}$$
$$\tau = \frac{\sigma_\theta - \sigma_r}{2} = \frac{\sigma_{ys}}{2}\left(\frac{c}{r}\right)^3, \quad (3)$$

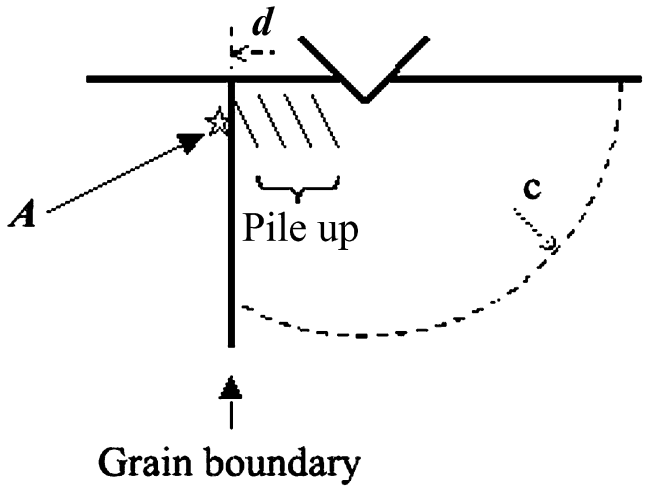

FIG. 8. Schematic illustration showing the elasto-plastic boundary c on the indented grain. Point A is a dislocation source on the neighboring grain.

where σ_r and σ_θ are the radial and hoop stresses respectively, τ is the maximum shear stress, and r is the radial distance from the indent center. In the original cavity model, Eq. (3) is applicable to the region $r \geq c$, but in the current picture of indenting near a grain boundary, as shown in Fig. 8, we assume that it is also applicable to the virgin neighboring grain up to the pop-in load.

Hence, at a point such as *A* at the grain boundary in the virgin grain, the maximum shear stress is

$$\tau \approx \frac{\sigma_{ys}}{2}\left(\frac{c}{d}\right)^3 \quad . \tag{4}$$

The condition for point *A* to emit dislocations to cause a subsequent avalanche can be described by

$$\tau\sqrt{r_o} = K_c \quad , \tag{5}$$

where r_o is the distance of the source at point *A* from the grain boundary, and K_c is a critical stress intensity factor for the emission, into which a misorientation factor between the maximum-shear-stress plane and the slip system in the virgin grain is absorbed. Hence, combining Eqs. (4) and (5), the condition for the avalanche to occur is estimated to be

$$\left(\frac{c}{d}\right)^3 \approx \frac{2K_c}{\sigma_{ys}\sqrt{r_o}} \quad . \tag{6}$$

A crude estimate of the source distance r_o can be approximately 0.1 μm, and $c/d \approx 1.5$ to 5 for different grain boundaries as observed in Fig. 3. Taking $\sigma_{ys} =$ 103 MPa,[19] K_c can be estimated to be approximately 0.05–2 $MPam^{1/2}$. This seems to be a wide range but it must be remembered that this is for different grain boundaries exhibiting a range of critical *c/d* ratios as shown in Fig. 3. The statistics in Fig. 3 show that some grain boundaries are many times more difficult to transmit slip than the others, but softer grain boundaries with lower K_c values seem to be more abundant. The K_c here is for shear stress [see Eq. (5)], and so it should be about 2 to 3 times smaller than the macroscopic Hall–Petch slope, taking an orientation factor into account. The Hall–Petch slope due to the lower K_c values here is therefore approximately 0.1 to 0.15 $MPam^{1/2}$, and this compares reasonably well with the experimental value of approximately 0.19 $MPam^{1/2}$ for strain-annealed Nb.[22] The analysis here is certainly crude and future work focusing on, for example, the relationship between the critical *c/d* ratio and grain boundary misorientation should be performed.

V. CONCLUSION

Using a Berkovich diamond indenter, the slip transmission behavior near grain boundaries was investigated in polycrystalline niobium. A type of strain burst induced by a nearby grain boundary during indentation was observed. The occurrence of this type of pop-in effect is found to be related to the misorientation across the grain boundary. The ratio of *c/d*, where *c* is the radius of the elasto-plastic boundary when the strain burst occurs, and *d* is the distance of indent center from the grain boundary, is found to be within a narrow range for a specific grain boundary segment, but it can vary between 1.5 and 5 for different grain boundaries.

ACKNOWLEDGMENT

The work described in this paper was supported by a grant from the Research Grants Council of the Hong Kong Special Administrative Region, China (Project No. HKU 7062/01E).

REFERENCES

1. K.T. Aust, R.E. Hanneman, P. Niessen, and J.H. Westbrook: Solute induced hardening near grain boundaries in zone refined metals. *Acta Metall.* **16,** 291 (1968).
2. T. Watanabe, S. Kitamura, and S. Karashima: Grain-boundary hardening and segregation in alpha-iron-tin alloy. *Acta Metall.* **28,** 455 (1980).
3. L.B. Harris, V.R. Howes, and N.G. Cutmore: Microhardness of NaCl bicrystals. *J. Am. Ceram. Soc.* **65,** 35 (1982).
4. Y.T. Chou, B.C. Cai, Jr., A.D. Romig, and L.S. Lin: Correlation between grain-boundary hardening and grain-boundary energy in niobium bicrystals. *Philos. Mag. A* **47,** 363 (1983).
5. Z.Q. Zhou and Y.T. Chou: Structure dependence of grain-boundary hardening in oriented niobium bicrystals. *J. Less. Comm. Met.* **114,** 323 (1985).
6. J.W. Wyrzykowski and M.W. Grabski: The Hall-Petch relation in aluminum and its dependence on the grain-boundary structure. *Philos. Mag. A* **53,** 505 (1986).
7. C.S. Lee, G.W. Han, R.E. Smallman, D. Feng, and J.K.L. Lai: The influence of boron-doping on the effectiveness of grain boundary hardening in Ni_3Al. *Acta Mater.* **47,** 1823 (1999).
8. P.C. Wo and A.H.W. Ngan: Investigation of slip transmission behavior across grain boundaries in polycrystalline Ni_3Al using nanoindentation. *J. Mater. Res.* **19,** 189 (2004).
9. G.K. Baranova: Etching of dislocations in niobium single-crystals. *Scripta Metall.* **11,** 827 (1977).
10. T.F. Page, W.C. Oliver, and C.J. McHargue: The deformation-behavior of ceramic crystals subjected to very low load (nano)indentations. *J. Mater. Res.* **7,** 450 (1992).
11. W.W. Gerberich, J.C. Nelson, E.T. Lilleodden, P. Anderson, and J.T. Wyrobek: Indentation induced dislocation nucleation: The initial yield point. *Acta Mater.* **44,** 3585 (1996).
12. S.A. Syed Asif and J.B. Pethica: Nanoindentation creep of single-crystal tungsten and gallium arsenide. *Philos. Mag. A* **76,** 1105 (1997).
13. D.F. Bahr, D.E. Kramer, and W.W. Gerberich: Non-linear deformation mechanisms during nanoindentation. *Acta Mater.* **46,** 3605 (1998).
14. T.A. Michalske and J.E. Houston: Dislocation nucleation at nanoscale mechanical contacts. *Acta Mater.* **46,** 391 (1998).
15. A. Gouldstone, H.J. Koh, K.Y. Zeng, A.E. Giannakopoulos, and S. Suresh: Discrete and continuous deformation during nanoindentation of thin films. *Acta Mater.* **48,** 2277 (2000).
16. Y.L. Chiu and A.H.W. Ngan: Time-dependent characteristics of incipient plasticity in nanoindentation of a Ni_3Al single crystal. *Acta Mater.* **50,** 1599 (2002).
17. Y.L. Chiu and A.H.W. Ngan: A TEM investigation on indentation

plastic zones in $Ni_3Al(Cr,B)$ single crystals. *Acta Mater*. **50,** 2677 (2002).
18. D. Kramer, H. Huang, M. Kriese, J. Robach, J. Nelson, A. Wright, D. Bahr, and W.W. Gerberich: Yield strength predictions from the plastic zone around nanocontacts. *Acta Mater*. **47,** 333 (1999).
19. K. Ishio, K. Kikuchi, M. Kusano, M. Mizumoto, K. Mukugi, A. Naito, N. Ouchi, and Y. Tsuchiya: Fracture toughness and mechanical properties of pure niobium and welded joints for superconducting cavities at 4K. In *Proceedings of the 9th Workshop on RF Superconductivity*, edited by B. Rusnak (Santa Fe, NM, 1999), Organized by Los Alamos National Laboratory, NM, Published online at http://lansce.lanl.gov/rfsc99/.
20. K.L. Johnson, *Contact Mechanics* (Cambridge University Press, Cambridge, U.K., 1985), pp. 173.
21. K. Zeng, E. Söderlund, A.E. Giannakopoulos, and D.J. Rowcliffe: Controlled indentation: A general approach to determine mechanical properties of brittle materials. *Acta Mater*. **44,** 1127 (1996).
22. P.R.V. Evans: The dependence of the lower yield stress on grain size in niobium. *J. Inst. Met*. **92,** 57 (1963).